Photoinduced Electron Transfer from Aromatic Aldehyde Hydrazones to Triplet States of C_{60} and C_{70}; Electron-Mediating and Hole-Shifting Systems

Osamu Ito,* Yoshiko Sasaki,† Mohamed E. El-Khouly, Yasuyuki Araki, Mamoru Fujitsuka, Akiko Hirao,†† and Hideyuki Nishizawa††

Institute of Multidisciplinary Research for Advanced Materials, Tohoku University, CREST, Japan Science and Technology Corporation (JST), Katahira, Sendai 980-8577

†Shokei Girl's High School, Hirose-machi, Aoba-ku, Sendai 980-0873

††Research Development Center, Toshiba Corp., Komukai, Saiwai-ku, Kawasaki 212-8582

(Received November 9, 2001)

Photoinduced electron transfer of fullerenes such as C_{60} and C_{70} in the presence of aromatic aldehyde hydrazones (AAH's) has been studied by the nanosecond laser photolysis which measures the transient absorption spectra in the visible and near-IR regions. Electron-transfer takes place from AAH's to the triplet states of fullerenes; the rates and efficiencies of electron transfer are strongly affected by the electron-donor ability of AAH's as evaluated by their oxidation potentials. The absorption bands of the radical cations of AAH's appeared in the near-IR reagion, indicating that the radical-cation center (hole) delocalizes in the entire region of each AAH. On addition of a viologen dication to C_{60}/C_{70}–AAH, the electron of the anion radical of fullerenes moves to viologen dication yielding the viologen radical cation. In the systems of octaethyl porphyrinatozinc (ZnOEP)–C_{60}/C_{70}–AAH, the hole shift was observed from the radical cation of ZnOEP, which was produced by photoinduced electron transfer from the triplet state of ZnOEP to C_{60}/C_{70}, to AAH.

Aromatic amines with highly π-electron delocalization are useful for the photoinduced charge-generating reagents and charge-mediating reagents in the electroluminescence devices, which attract much attention because of technological uses.[1] Recently, it has been pointed out that fullerenes act as good electron acceptors in photoinduced electron-transfer processes.[2–5] Because of high delocalization of the π-electrons in fullerenes, the transient absorption bands due to the excited singlet states, triplet states, and anion radicals appear in the near-IR region.[6–8] In addition, absorption bands of the radical cations of such highly π-delocalized aromatic amines would be anticipated in the longer wavelengths. Thus, it is indispensable to measure the transient spectra in the visible and near-IR regions in order to disclose the routes and rates of the generations and movements of electrons and holes.

As paths of photoinduced electron-transfer processes of fullerenes in the presence of aromatic amines, it has been reported that the excited states of fullerenes accept the electron from the electron-donors in their ground states.[6–8] The relative contributions of the singlet states and the triplet states of fullerenes to the photoinduced electron-transfer process vary with concentration of donors. Since the intersystem crossing processes of C_{60} and C_{70} are as fast as 10^9 s^{-1},[9–11] the excited singlet route can be achieved only at high concentrations of donors,[12,13] while the triplet route is favorable at low concentrations of donors.[14,15]

We report here that the efficiencies and rates of the photoinduced electron transfer can be easily evaluated with the decay of the excited states and the rise of the anion radicals of fullerenes in the presence of aldehyde hydrazone derivatives (–CH=N–N< (**1** – **4**) and >C=CH–CH=N–N< (**5**)), as shown in Scheme 1.[16–18] The π-conjugations in the aldehyde hydrazone moiety would be extended by the substitution with the aromatic amine moieties such as aniline, carbazole, and tetrahydroquinoline. Thus, such highly π-conjugated molecules can be used as charge-generating and charge-transferring materials in the electroluminescence devices.[16–18] The rates and quantum yields for the electron-transfer processes via the triplet states of C_{60} ($^3C_{60}$*) and C_{70} ($^3C_{70}$*) were compared by changing the structure of aromatic aldehyde hydroazones (AAH's).

Furthermore, we investigate the addition effect of viologen dication; in such systems, the radical anions of C_{60} and C_{70} ($C_{60}^{\bullet-}$ and $C_{70}^{\bullet-}$) can mediate their electrons to the viologen dication. This reveals that an efficient photosensitizing electron-transfer/electron-mediating system will be established upon photoexcitation of the fullerenes. Furthermore, the role of such AAH's as hole-shifting reagents is examined in the photoinduced charge-separation systems to establish an efficient photosensitizing electron-transfer/hole-shifting system. We expect that the donor ability and hole-shifting ability of AAH's would vary with the changes of the structure of AAH's, which accompany the changes in the electronic properties.

Experimental

Materials. C_{60} and C_{70} were obtained from Texas Fullerenes Corporation at a purity of 99.9 and 99%, respectively. The aro-

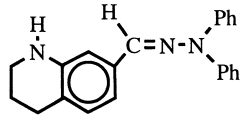

1; 1,2,3,4-tetrahydroquinolin-7-carbadehyde dephenyl-hydrazone

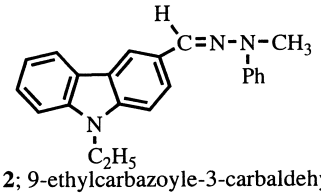

2; 9-ethylcarbazoyle-3-carbaldehyde *N*-methyl-*N*-phenyl hydrazone

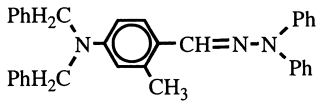

3; 4-(dibenzylamino-2-methylbenzaldehyde diphenylhydrazone

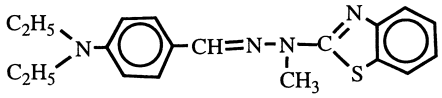

4; 4-diethylaminobenzaldehyde *N*-(benzothiazol-2-yl)-*N*-methylhydrazone

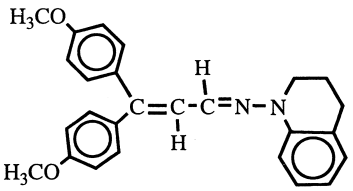

5; 1-[3,3'-bis(4-methoxyphenyl)allylideneamino]-1,2,3,4-tetrahydroquinoline

C_{60}

C_{70}

Scheme 1.

matic aldehyde hydrazones (AAH's) employed in the present study were all commercially available: **1** and **3** from Anan Koryo LTD, Japan and **2**, **4**, and **5** from Inui Regents LTD, Japan. Octylviologen dication (OV^{2+}) was used as perchlorate. Octaethyl porphyrinatozinc (ZnOEP) was obtained from Aldrich. Benzonitrile (PhCN) used as solvent was of HPLC grade.

Apparatus. Oxidation potentials (E_{ox}) of AHH's were measured by a voltammetric analyzer (BAS CV-50W) in a conventional three electrode-cell equipped with Pt-working and counter electrodes with an Ag/AgCl reference electrode at scan rate of 100 mV/s. In each case, the solution contained $(1.0 - 5.0) \times 10^{-3}$ mol dm^{-3} of a sample with 0.1 mol dm^{-3} of tetrabutylammonium perchlorate (Nakarai Tesque); the solution was deaerated with Ar-bubbling before measurements. These E_{ox} values are summarized in Table 1.

Steady-state absorption spectra were measured with a JASCO/V-570 spectrophotometer. The steady-state absorption spectra of the radical cations were observed by the step-wise addition of $FeCl_3$ to the AAH solutions.[19]

Transient absorption spectra in the visible and near-IR regions were observed by the laser-flash photolysis apparatus. In the systems of C_{60}/C_{70}–hydrazones and C_{60}/C_{70}–hydrazones–OV^{2+}, C_{60} and C_{70} were excited with the SHG (532 nm) light of a Nd:YAG laser (Quanta-Ray; 6 ns fwhm). In the systems of ZnOEP–C_{60}/C_{70}–AAH, ZnOEP absorbs more than 90% of the laser light at 532 nm. For time-scale measurements shorter than 10 μs, a Si-PIN photodiode module (400 – 600 nm) and a Ge-APD module (600 – 1600 nm) were employed as detectors for monitoring the light from a pulsed Xe-lamp.[19,20] For time-scale measurements longer than 10 μs, an InGaAs-PIN photodiode was used as a detector for monitoring light from a continuous Xe-lamp (150 W).[19,20] The sample solutions were deaerated by bubbling with Ar gas before measurements. The laser photolysis was performed for the solution in a rectangular quartz cell with a 10 mm optical path. All the measurements were carried out at 23 °C. Details of the experimental procedures are described elsewhere.[19,20]

Table 1. Oxidation Potentials (E_{ox}) of AAH and Absorption Maxima (λ_{max}) and Molar Extinction Coefficients (ε_c) of Radical Cations of AAH in PhCN

AAH-Donors	E_{ox} [a] /V	Radical Cations	λ_{max} /nm	ε_c [b] /mol^{-1} dm^3 cm^{-1}	Δ_{MO} [c] /eV
1	0.66	$\mathbf{1}^{\bullet+}$	520	10000	
			1100	9500	0.4241
2	0.84	$\mathbf{2}^{\bullet+}$	470	25000	
			1070	6700	0.3906
3	0.75	$\mathbf{3}^{\bullet+}$	540	20000	
			1080	14000	0.5175
4	0.77	$\mathbf{4}^{\bullet+}$	450	13000	
			940	11000	0.2669
5	0.67	$\mathbf{5}^{\bullet+}$	620	25000	
			880	14500	0.5907

a) Calculated as vs. SCE.
b) The ε_c values were evaluated on comparison with that of $C_{70}^{\bullet-}$ (4000 mol^{-1} dm^3 cm^{-1} at 1380 nm).
c) Δ_{MO} is energy gap between HOMO and next HOMO, which corresponds to the longest absorption maximum of each radical cation of AAH.

Molecular Orbital Calculation. The energy levels and electron densities of neutral donor molecules and the unpaired electron densities of the radical cations were calculated with PM3 method in MOPAC-2000 after the geometries of neutral molecules and radical cations were optimized separately,[21] because the two geometries are slightly different.

Results and Discussion

Steady-State UV/Visible Spectra. The steady-state absorption spectra of **2**, C_{60} and their mixture in PhCN are shown in Fig. 1. The absorption spectrum of the mixture of C_{60} and **2** in PhCN is almost the same as the calculated spectrum by add-

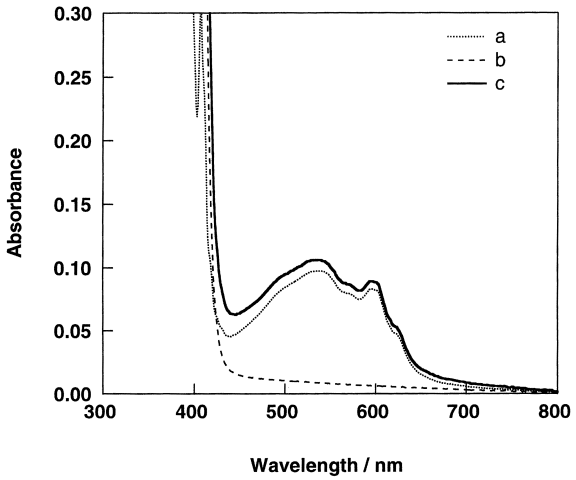

Fig. 1. Steady-state absorption spectra of (a) C_{60} (0.1×10^{-3} mol dm^{-3}), (b) **2** (1.0×10^{-3} mol dm^{-3}), and (c) their mixture in PhCN.

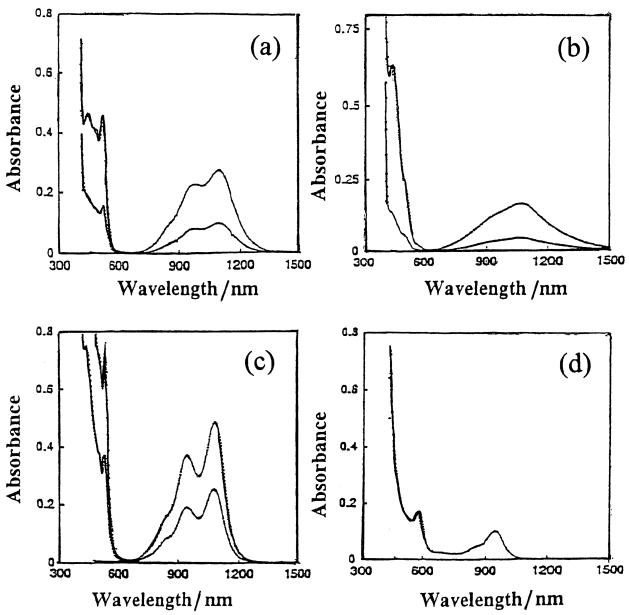

Fig. 2. Steady-state absorption spectra observed on addition of $FeCl_3$ to AAH's in PhCN; (a) **1**, (b) **2**, (c) **3**, and (d) **5**.

ing C_{60} and **2**. This finding suggests that no appreciable interaction exists between C_{60} and **2** in the ground state. For other C_{60}–AAH and C_{70}–AAH systems in PhCN, spectral features of the mixtures are similar to those of the summed spectra of the constituents.

AAH's have main absorptions in the shorter wavelength region with a weak absorption tail up to 800 nm, as shown in Fig. 1 for **2** as an example. On excitation of AAH in PhCN with the 532 nm-laser light, appreciable transient absorption bands were not observed. Thus, it is presumed that the laser light at 532 nm predominantly excites C_{60}.

The steady-state absorption spectra of the radical cations of AAH's employed as electron–donors were observed by chemical oxidation with $FeCl_3$ in PhCN, as shown in Fig. 2. The absorption maxima (λ_{max}) of the radical cations of AAH's are

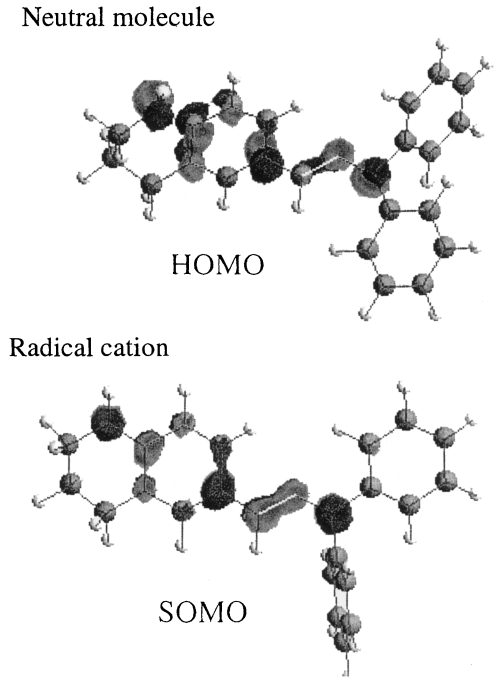

Fig. 3. Electron densities of HOMO of neutral molecule (**1**) and unpaired electron density of SOMO of $\mathbf{1}^{\bullet+}$.

summarized in Table 1, in which the molar extinction coefficients (ε_c) of the radical cations were evaluated on the basis of the molar extinction coefficient of $C_{70}^{\bullet-}$ (ε_A = 4000 mol^{-1} dm^3 cm^{-1} at 1380 nm) observed by the laser flash photolysis as described in the next section.[22,23]

The transition energies of the near-IR absorption bands of the radical cations of AAH's may correspond to the energy gap (Δ_{MO}) between HOMO and next HOMO of each neutral molecule as listed in Table 1. Although the observed transition energies are slightly smaller than the corresponding calculated energy gaps, it has been shown that the radical cations have quite small transition energies due to the delocalization of the electrons (or holes) in AAH's.

MO pattern of HOMO of **1** is shown in Fig. 3 for example. The electron in HOMO is delocalized mainly on the aldehyde hydrazone moiety; the electron distrubution is also present at the N-atoms of the aniline moiety attached to the aldehyde hydrazone moiety.

The half-occupied electron distribution of SOMO of the radical cation (hole) is also shown in Fig. 3; the optimized structure of the radical cation calculated with PM3 is slightly different from that of the neutral molecule. The holes are quite widely distributed over whole aldehyde hydrazone moiety including the aniline moiety, similar to the electron distribution of HOMO of the neutral molecule.

Transient Spectra in PhCN. Figure 4 shows the nanosecond transient spectra observed by the laser excitation of C_{60} in the visible and near-IR regions in the presence of **3** in PhCN. The absorption band of $^3C_{60}$* at 740 nm,[3–6] which appeared immediately after the laser exposure, began to decay in the presence of **3**. Along with the decay of $^3C_{60}$*, the absorption intensity at 1080 nm increased, which suggests that $C_{60}^{\bullet-}$ and the radical cation of **3** ($\mathbf{3}^{\bullet+}$) are formed via $^3C_{60}$* accepting an

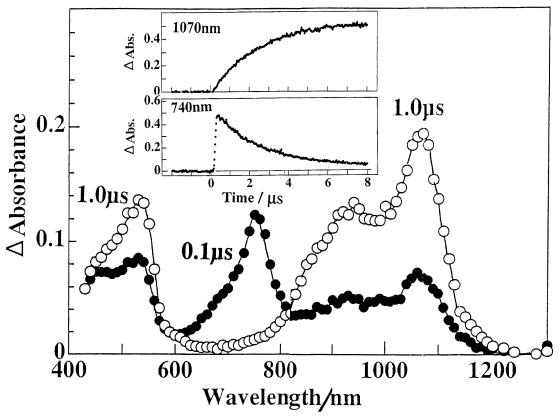

Fig. 4. Transient absorption spectra obtained by 532 nm laser light excitation of C_{60} (0.1×10^{-3} mol dm^{-3}) in the presence of **3** (1×10^{-3} mol dm^{-3}) in deaerated PhCN. Inset: Time profiles at 740 and 1070 nm for the mixture of C_{60} (0.1×10^{-3} mol dm^{-3}) and **3** (1.0×10^{-3} mol dm^{-3}).

electron from **3**.[3–6] The absorption bands at 520 nm and 950 nm appearing after the decay of $^3C_{60}$* can be attributed to $\mathbf{3}^{\bullet+}$ from the comparison with the steady-state absorption spectrum of $\mathbf{3}^{\bullet+}$ (Fig. 2). At 1080 nm, the absorption band of $C_{60}^{\bullet-}$ is overlapping with that of $\mathbf{3}^{\bullet+}$.

The time profiles for the decay of $^3C_{60}$* at 740 nm and the rises of $C_{60}^{\bullet-}$ and $\mathbf{3}^{\bullet+}$ at 1080 nm are shown in Fig. 4. The decay curve of $^3C_{60}$* and rise curves of $C_{60}^{\bullet-}$ and $\mathbf{3}^{\bullet+}$ are almost mirror images, supporting the conclusion that electron transfer takes place via $^3C_{60}$* as shown in Scheme 2, in which k_{ics}, k_{et}, k_{cq}, and k_{bet} are the rate constants of the intersystem crossing, electron transfer, collisional quenching, and back electron transfer, respectively. The observed slow rises of $C_{60}^{\bullet-}$ and $\mathbf{3}^{\bullet+}$ indicate clearly that electron transfer does not take place via $^1C_{60}$*. The contribution of $^1C_{60}$* to the formations of the radical ions would be anticipated by further addition of AAH's; however, additions of the high concentration of AAH's

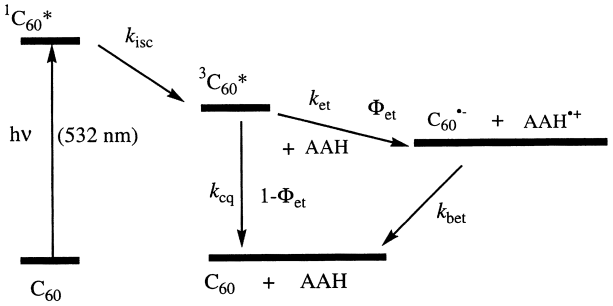

Scheme 2.

to C_{60} in PhCN prohibited the observation of the radical ions, probably because of formation of the exciplexes, which do not dissociate into the radical ions.

Each decay of $^3C_{60}$* at 740 nm obeys first-order kinetics (Fig. 4), yielding the first-order rate constant (k_{1st}). The k_{1st} value increases linearly with the concentration of AAH donor. The second-order quenching rate constants (k_q) of $^3C_{60}$* by AAH donors can be obtained from the slopes of the pseudo-first-order plots as listed in Table 2. These k_q values do not vary much with changing AAH's, falling in a narrow range of $(2.8 - 3.6) \times 10^9$ mol^{-1} dm^3 s^{-1}.

The transient absorption spectra of C_{70} in the presence of **5** are shown in Fig. 5. The transient absorption band of $^3C_{70}$* at 940 – 980 nm appeared immediately after the laser-light exposure; then the absorption intensity of $C_{70}^{\bullet-}$ at 1380 nm increased after 1.0 μs. The observed time-profiles of the absorption bands of $^3C_{70}$* and $C_{70}^{\bullet-}$ are quite similar to those in Fig. 4, except that the decay of $^3C_{70}$* at 980 nm seems to be slower because of the overlap with the rise of $\mathbf{5}^{\bullet+}$. Since the rise rate of $C_{70}^{\bullet-}$ is similar to the decay rate of $^3C_{70}$*, the $C_{70}^{\bullet-}$ is produced via $^3C_{70}$* accepting an electron from **5**. The k_q values evaluated from the rise rate of $C_{70}^{\bullet-}$ are summarized in Table 2. The k_q values evaluated for the C_{70}–AAH systems are almost identical with those for the corresponding C_{60}–AAH sys-

Table 2. Free-Energies ($\Delta G°_{et}$), Rate Constants for Quenching (k_q), Quantum Yields (Φ_{et}), Rate Constants (k_{et}) for Electron-Transfer from AAH to $^3C_{60}$* and $^3C_{70}$*, and Back Electron-Transfer Rate Constants (k_{bet}) from $C_{60}^{\bullet-}$ ($C_{70}^{\bullet-}$) to $[AAH]^{\bullet+}$ in PhCN

AAH donors	Fullerene acceptors	$\Delta G°$ /kJ mol^{-1}	k_q[a] /mol^{-1} dm^3 s^{-1}	Φ_{et}	k_{et} /mol^{-1} dm^3 s^{-1}	k_{bet}[b] /mol^{-1} dm^3 s^{-1}
1	C_{60}	−46.0	2.9×10^9	0.37	1.7×10^9	3.0×10^9
1	C_{70}	−50.8	3.1×10^9	0.35	1.1×10^9	5.2×10^9
2	C_{60}	−28.5	2.8×10^9	0.73	2.0×10^9	5.5×10^9
2	C_{70}	−33.2	3.3×10^9	0.63	2.1×10^9	4.0×10^9
3	C_{60}	−37.3	3.4×10^9	0.96	3.3×10^9	2.8×10^9
3	C_{70}	−42.1	4.8×10^9	0.70	3.4×10^9	3.7×10^9
4	C_{60}	−35.3	3.6×10^9	0.39	1.4×10^9	3.0×10^9
4	C_{70}	−40.1	3.9×10^9	0.30	1.2×10^9	4.6×10^9
5	C_{60}	−45.0	3.2×10^9	0.28	9.0×10^8	4.7×10^9
5	C_{70}	−49.8	3.3×10^9	0.25	8.3×10^8	5.4×10^9

a) The k_q values for C_{60} were evaluated from the decay of $^3C_{60}$*, while the k_q values for C_{70} were evaluated from the rise of decay of $C_{70}^{\bullet-}$; both values contain estimation error of about ±5%.

b) The k_{bet} values were evaluated using the ε_c values in Table 1; each k_{bet} value contains estimation error of about ±5%.

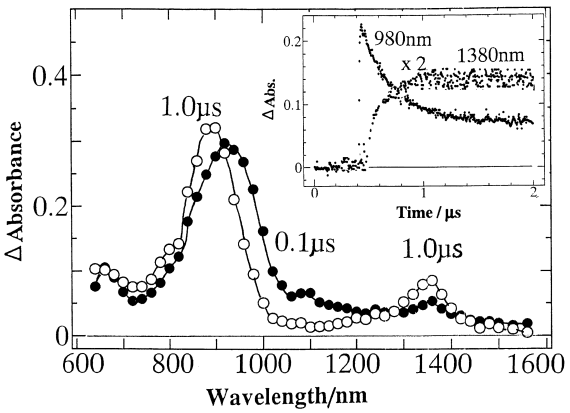

Fig. 5. Transient absorption spectra obtained by 532 nm laser light of C_{70} ($0.1 \times$ mol dm^{-3}) in the presence of **5** (1×10^{-3} mol dm^{-3}) in PhCN. Inset: Time profiles at 980 and 1380 nm.

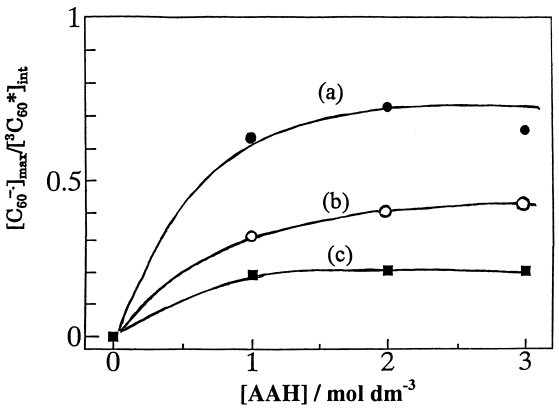

Fig. 6. Plots of efficiencies of electron transfer $[C_{60}^{\bullet-}]_{max}/[^3C_{60}^*]_{int}$ vs [AAH]; (a) **2**, (b) **4**, and (c) **5**.

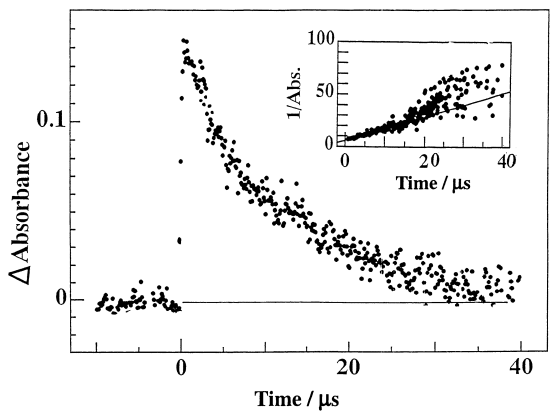

Fig. 7. Long time-scale decay of $C_{70}^{\bullet-}$ produced by electron transfer from **2** in PhCN (at 1380 nm). Inset: Second-order plot.

tems.

Quantum Yields and Rates for Electron Transfer. In the case of C_{60}–AAH systems, the efficiency of electron transfer via $^3C_{60}^*$ can be obtained from the ratio of the initial maximal absorbance of $^3C_{60}^*$ at 740 nm to the maximal absorbance of $C_{60}^{\bullet-}$ at 1080 nm, $[C_{60}^{\bullet-}]_{max}/[^3C_{60}^*]_{int}$. As shown in Fig. 6, such ratios show saturation with increasing AAH donors. At sufficiently high concentration of AAH donors above ca. 3×10^{-3} mol dm^{-3}, the efficiency can be put equal to the quantum yield (Φ_{et}) of the electron transfer process via $^3C_{60}^*/^3C_{70}^*$ (Table 2).[15,22] When the absorption band of $C_{60}^{\bullet-}$ was overlapping with the bands of the radical cation, the absorbance due to the radical cation was subtracted by using the ε_c values in Table 1. The observed order of Φ_{et} is **3** > **2** > **4** ≥ **1** > **5**.

In the case of C_{70}–AAH systems, the Φ_{et} values were similarly evaluated after subtraction of the absorbance of the radical cation from the absorbances of $^3C_{70}^*$ and $C_{70}^{\bullet-}$. The Φ_{et} values of the C_{70}–AAH systems are slightly smaller than the corresponding values for C_{60}. The observed order of Φ_{et} is **3** > **2** > **1** ≥ **4** > **5**, which is quite similar to that for C_{60}.

Since all Φ_{et} values in Table 2 are less than 1.0, there are quenching processes other than electron transfer; in Scheme 2, these processes are described as collisional quenching processes, which may include deactivation via encounter complexes ($^3C_{60}^*/^3C_{70}^*\cdots$AAH) and exciplexes [$^3(C_{60}^{\delta-}/C_{70}^{\delta-}\cdots AAH^{\delta+})^*$] without forming the radical ions which persist more than ca. 10 ns.

Finally, the electron-transfer rate constants (k_{et}) can be obtained from the relation of $k_{et} = \Phi_{et}\, k_q$ as listed in Table 2.[15,22] Thus, the k_{et} values in the range of $(0.8 - 3.3) \times 10^9$ mol^{-1} dm^3 s^{-1} were evaluated; these are slightly smaller than the value at the diffusion controlled limit ($k_{diff} = 5.2 \times 10^9$ mol^{-1} dm^3 s^{-1} in PhCN).[24] The observed order of k_{et} is **3** > **2** > **1** > **4** > **5** for C_{60}, which is almost same as that for C_{70}, except for **4** ≥ **1**. These orders of the k_{et} values reflect the order of Φ_{et} rather than that of k_q.

From the Rehm–Weller equation,[25] the free-energy changes (ΔG°_{et}) can be calculated for the electron-transfer systems between $^3C_{60}^*/^3C_{70}^*$ and AAH donors in PhCN by employing the T_1-energy levels of $^3C_{60}^*$ (= 1.53 eV)[26] and $^3C_{70}^*$ (= 1.50 eV),[27] the reduction potentials (E_{red}) of C_{60} (−0.51 V vs SCE)[28] and C_{70} (−0.43 V vs SCE),[29] the oxidation potentials (E_{ox}) of AAH's (Table 1), and the Coulomb energy (0.06 eV).[4] These ΔG°_{et} values listed in Table 2 are all sufficiently negative to support the nearly diffusion-controlled rate constants for the electron-transfer processes. The order of these $-\Delta G^\circ_{et}$ values is **1** ≥ **5** > **3** ≥ **4** > **2**, reflecting the order of the E_{ox} values of AAH's. However, these orders are not always similar to those of Φ_{et} and k_{et}. Factors other than ΔG°_{et} may control the orders of Φ_{et} and k_{et}, although such factors are not clarified in the present stage.

Back Electron Transfer. The $C_{70}^{\bullet-}$ begins decaying after reaching the maximum intensity, as shown in Fig. 7 in a longer time scale. The second-order plot (1/ΔAbs vs time) for the decay of $C_{70}^{\bullet-}$ shows a linear relation in the initial stage (inset of Fig. 7); the later stage may contain much noise. Observed second-order kinetics indicates a bimolecular reaction, probably by recombination of $C_{70}^{\bullet-}$ with $\mathbf{2}^{\bullet+}$ in the same concentration, yielding neutral molecules in their ground states (in Scheme 2). The bimolecular second-order kinetics also suggests that the back electron transfer takes place after the radical cation and radical anion were separately solvated as free radical ions. The slope of the second-order plot is attributed to k_{bet}/ε_A. On substituting the reported ε_A at 1380 nm for $C_{70}^{\bullet-}$, one can cal-

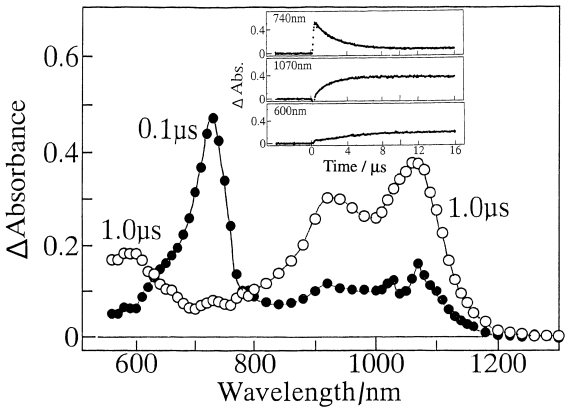

Fig. 8. Transient absorption spectra obtained by 532 nm laser light excitation of C_{60} (0.1×10^{-3} mol dm^{-3}) in the presence of **2** (1×10^{-3} mol dm^{-3}) and OV^{2+} (1×10^{-3} mol dm^{-3}) in PhCN. Inset: Time profiles at 740, 1070, and 600 nm.

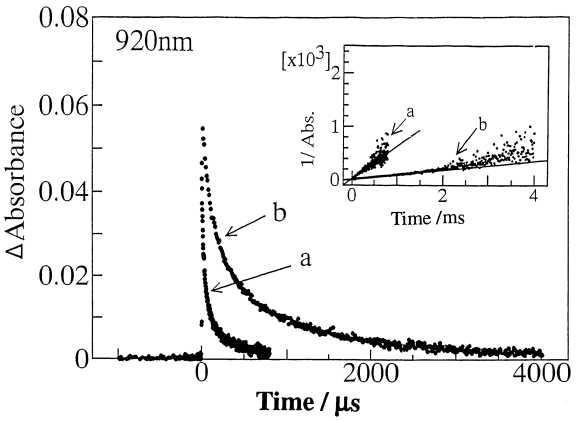

Fig. 9. Long time-scale decays of [$\mathbf{2}^{\bullet+}$] at 920 nm produced via $^3C_{60}$* in PhCN; (a) in the absence of OV^{2+} and (b) in the presence of OV^{2+}. Inset: Second order plots.

culate the k_{bet} values as listed in Table 2. In the case of $C_{60}^{\bullet-}$, the k_{bet} values were similarly evaluated from the decays of the radical cations of AAH's using the ε_c values listed in Table 1, because of overlapping of the absorption band of $C_{60}^{\bullet-}$ with those of $AAH^{\bullet+}$. The k_{bet} values for $C_{60}^{\bullet-}$ are almost the same as those of $C_{70}^{\bullet-}$. They are in the range of $(2.8 - 5.5) \times 10^9$ mol^{-1} dm^3 s^{-1}, which are all quite near to the k_{diff} value in PhCN. Although $k_{bet} > k_{et}$, the rate of the forward reaction is faster than that of the backward reaction, because the concentration of AAH is much higher than that of $AAH^{\bullet+}$, even though the concentration of $C_{60}^{\bullet-}$ ($C_{70}^{\bullet-}$) is similar to that of $^3C_{60}$* ($^3C_{70}$*).

Electron-Mediating System. When octylviologen dication (OV^{2+}), which is a well-known electron-mediating reagent,[9] was added to the mixture of C_{60} and **2**, the transient absorption spectra were observed by the laser light excitation of C_{60}; these are shown in Fig. 8. Along with the rapid decay of $^3C_{60}$* and the rises of $C_{60}^{\bullet-}$ and $\mathbf{2}^{\bullet+}$, $OV^{\bullet+}$ appeared at 600 nm. The rise rate of $OV^{\bullet+}$ was slower than those of $C_{60}^{\bullet-}$ and $\mathbf{2}^{\bullet+}$, as shown in Fig. 8. In the case of C_{70}/AAH/OV^{2+} system, the rise of $OV^{\bullet+}$ was observed after the decay of $C_{70}^{\bullet-}$ at 1380 nm. These observations suggest that $OV^{\bullet+}$ is produced by transfer of an electron from $C_{60}^{\bullet-}$/ $C_{70}^{\bullet-}$ to OV^{2+}, which is referred to as the electron-mediating process.[9] Thus, the photosensitized electron-transfer/electron-mediating system was established with the photoexcitation of fullerenes (C_{60}/C_{70}) as shown in Scheme 3, in which k_{md} and k_{fbet} are the rate constants

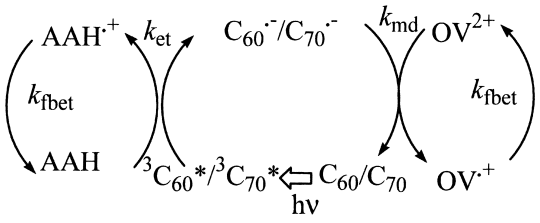

Electron-mediating system

Scheme 3.

of the electron-mediating process and of the final back electron-transfer process from $OV^{\bullet+}$ to $AAH^{\bullet+}$, respectively. The k_{md} value was evaluated to be 2.5×10^9 mol^{-1} dm^3 s^{-1} in PhCN from the rise of $OV^{\bullet+}$ with changing the concentration of OV^{2+}, since the k_{md} value can not be evaluated from the decay of the absorption band of $C_{60}^{\bullet-}$ at 1080 nm due to the overlap with the broad absorption band of $AAH^{\bullet+}$ in the 900–1100 nm region.

The decay time-profiles of $\mathbf{2}^{\bullet+}$ at 920 nm in the presence and absence of OV^{2+} are shown in Fig. 9. The decay rate of $\mathbf{2}^{\bullet+}$ in the presence of OV^{2+} is slower than that in the absence of OV^{2+}. The slope of the second-order plot of $\mathbf{2}^{\bullet+}$ (or $OV^{\bullet+}$) gave $k_{fbet} = 4.3 \times 10^8$ mol^{-1} dm^3 s^{-1}, while the slope in the absence of OV^{2+} gave $k_{bet} = 5.5 \times 10^9$ mol^{-1} dm^3 s^{-1} (Table 2). This finding indicates that the lifetime of $\mathbf{2}^{\bullet+}$ becomes longer compared with the electron-transfer process between oppositely charged species $\mathbf{2}^{\bullet+}$and $C_{60}^{\bullet-}$, suggesting that the rate of the electron-transfer process between the positively charged species ($\mathbf{2}^{\bullet+}$ and $OV^{\bullet+}$) slows down due to the repulsion.

Hole-Shifting System. In order to investigate the hole-shifting ability of AAH, ZnOEP was selectively photoexcited in the presence of C_{70} and **1** in PhCN as shown in Fig. 10. The strong absorption band at 440 nm that appeared immediately after the laser pulse was attributed to the triplet state of ZnOEP (^{3}ZnOEP*); the weak absorption at 760 nm was also ascribed to ^{3}ZnOEP*. The absorption of $^3C_{70}$* was not observed at 980 nm in the spectrum at 0.5 μs, indicating that the selective excitation of ZnOEP was almost complete. With the decay of ^{3}ZnOEP* at 440 nm, the rise of $C_{70}^{\bullet-}$ was observed at 1380 nm. These observations indicate that $ZnOEP^{\bullet+}$ and $C_{70}^{\bullet-}$ are produced by photoinduced electron transfer from ^{3}ZnOEP* to C_{70}.[33] Although the formation of the radical cation of ZnOEP ($ZnOEP^{\bullet+}$) was confirmed by the absorption at 680 nm that appeared at the transient spectrum at 0.5 μs, $ZnOEP^{\bullet+}$ disappeared at 5 μs in the presence of **1**. Concomitantly, the rise of the broad absorption in the 900 –1200 nm region of $\mathbf{1}^{\bullet+}$ appeared. In the time profiles, the rise of $\mathbf{1}^{\bullet+}$ at 1000 nm was slower than that of $C_{70}^{\bullet-}$, which suggests that the hole of $ZnOEP^{\bullet+}$ shifts to **1**, yielding $\mathbf{1}^{\bullet+}$ as shown in Scheme 4, in which k_{hs} is a rate constant of the hole-shift process.

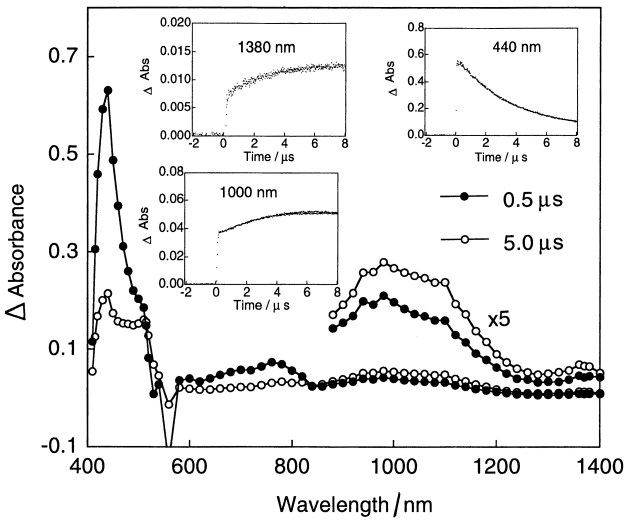

Fig. 10. Transient absorption spectra obtained by 532 nm laser light excitation of ZnOEP (0.1×10^{-3} mol dm^{-3}) in the presence of C_{70} (0.1×10^{-3} mol dm^{-3}) and **1** (4×10^{-3} mol dm^{-3}) in deaerated PhCN. Inset: Time profiles at 440, 1000, and 1380 nm.

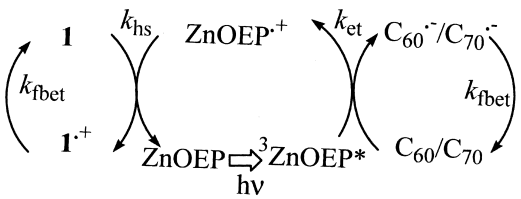

Hole-shift system

Scheme 4.

From the dependence of the rise rates of $\mathbf{1}^{\bullet+}$ at 1000 nm on the concentration of **1**, the k_{hs} value was evaluated to be 2.0×10^8 mol^{-1} dm^3 s^{-1}. Such a hole shift is possible when the E_{ox} values of AAH's are lower (less positive) than that of ZnOEP (E_{ox} = 0.72 V vs SCE).[34] Indeed, for AHH's with higher E_{ox} than that of ZnOEP, no hole shift was observed. In the case of hole shift, the k_{fbet} was evaluated from the long time-scale decay measurements $C_{60}^{\bullet-}/C_{70}^{\bullet-}$; however, the k_{fbet} value was almost the same as the k_{bet} value evaluated from the decay of $C_{60}^{\bullet-}/C_{70}^{\bullet-}$ in the absence of **1**.

Summary

Fullerenes (C_{60} and C_{70}) act as good photosensitizers and good electron acceptors in the presence of AAH donors for both are rich in delocalized π-electrons. Their transient species, such as triplet excited state and ion radicals, were well followed by the transient absorption spectra in the visible and near-IR regions, although accidental overlapping of the absorption band of $C_{60}^{\bullet-}$ with $AAH^{\bullet+}$ disturbed the analysis of rates and efficiency of electron transfer. The delocalization of radical-cation centers (holes) was elucidated from their near-IR bands and MO calculations. On addition of a viologen dication, the photosensitized electron-transfer/electron-mediating cycle was established, producing prolonged lifetimes of the holes of AAH's. The hole-shift ability of AAH from $ZnOEP^{\bullet+}$ was also proved in the photoinduced electron-transfer system from ^{3}ZnOEP* to C_{60}/C_{70}.

References

1 M. Pope and C. E. Swenberg, "Electronic Processes in Organic Crystals and Polymers," Second Ed., Oxford, New York (1999), pp.1182–1229.

2 K. Tanigaki, T. W. Ebbesen, and S. Kuroshima, *Chem. Phys. Lett.*, **185**, 189 (1991).

3 M. Maggini and D. M. Guldi, "Molecular and Supramolecular Photochemistry," ed by V. Ramamurthy and K. S. Schanze, Marcel Dekker, New York (2000), Vol. 4, pp. 149–196.

4 D. M. Guldi and P. V. Kamat, "Fullerenes, Chemistry, Physics and Technology," ed by K. M. Kadish and R. S. Ruoff, Wiley-Interscience, New York (2000), pp. 225–281.

5 O. Ito, *Res. Chem. Intermed.*, **23**, 389 (1997).

6 J. W. Arbogast and C. S. Foote, *J. Am. Chem. Soc.*, **113**, 8886 (1991).

7 R. J. Senior, A. Z. Szarka, G. R. Smith, and R. M. Hochstrasser, *Chem. Phys. Lett.*, **185**, 179 (1991).

8 S. Fukuzumi, T. Suenobu, M. Patz, T. Hirasaka, S. Itoh, M. Fujitsuka, and O. Ito, *J. Am. Chem. Soc.*, **120**, 8060 (1998).

9 H. Onodera, Y. Araki, M. Fujitsuka, S. Onodera, O. Ito, F. Bai, M. Zheng, and J.-L Yang, *J. Phys. Chem. A*, **105**, 7341 (2001).

10 M. Gevaert and P. V. Kamat, *J. Phys. Chem.*, **96**, 9883 (1992).

11 A. Watanabe, O. Ito, M. Watanabe, H. Saito, and M. Koishi, *J. Phys. Chem.*, **100**, 10518 (1996).

12 J. Park, D. Kim, Y. D. Suh, and S. K. Kim, *J. Phys. Chem.*, **98**, 12715 (1994).

13 H. N. Ghosh, H. Pal, A. V. Sapre, and J. P. Mittal, *J. Am. Chem. Soc.*, **115**, 11722 (1993).

14 J. W. Arbogast, C. S. Foote, and M. Kao, *J. Am. Chem. Soc.*, **114**, 2277 (1992).

15 C. A. Steren, H. von Willigen, L. Biczok, N. Gupta, and H. Linschitz, *J. Phys. Chem.*, **100**, 8920 (1996).

16 S. Nomura, K. Nishimura, and Y. Shirota, *Thin Solid Films*, **273**, 27 (1996).

17 S. Nomura and Y. Shirota, *Chem. Phys. Lett.*, **268**, 461 (1997).

18 S. Nomura, K. Nishimura, and Y. Shirota, *Mol. Cryst. Liq. Cryst. Sci. Technol., Sect. A*, **313**, 249 (1998).

19 K. Matsumoto, M. Fujitsuka, T. Sato, S. Onodera, and O. Ito, *J. Phys. Chem.*, **104**, 11632 (2000).

20 T. Konishi, M. Fujitsuka, O. Ito, Y. Toba, and Y. Usui, *J. Phys. Chem. A*, **103**, 9938 (1999).

21 J. J. Stewart, *QCPE Bull.*, **9**, 10 (1989).

22 M. M. Alam, A. Watanabe, and O. Ito, *Bull. Chem. Soc. Jpn.*, **70**, 1833 (1997).

23 M. M. Alam, O. Ito, N. Sakurai, and H. Moriyama, *Res. Chem. Intermed.*, **25**, 323 (1999).

24 S. l. Murov, I. Carmichael, and G. L. Hug, "Handbook of Photochemistry," Marcel Dekker, 2nd ed, New York (1993).

25 D. Rehm and A. Weller, *Isr. J. Chem.*, **8**, 259 (1970).

26 R. R. Hung and J. J. Grabowski, *J . Phys. Chem.*, **95**, 6073 (1991).

27 R. E. Haufler, J. Conceicao, L. P. F. Chibante, Y. Chai, N. E. Byrne, S. Flanagan, M. M. Haley, S. C. O'Brien, C. Pan, Z. Xiao, W. E. Billups, M. A. Ciufolini, R. H. Hauge, J. L. Margrave,

L. J. Wilson, R. Curl, and R. E. Smally, *J . Phys. Chem.*, **94**, 8634 (1990).

28 P. M. Allemand, A. Koch, F. Wudl, Y. Rubin, F. Diederich, M. M. Alvarez, S. J. Anz, and R. L. Whetten, *J. Am. Chem. Soc.*, **113**, 1050 (1991).

29 D. Dubois, K. M. Kadish, S. Flanagan, R. E. Haufler, L. P. F. Chibante, and L. J. Wilson, *J. Am. Chem. Soc.*, **113**, 4364 (1991).

30 K. C. Hwang and D. Mauzerall, *Nature*, **361**, 138 (1993).

31 D. S. Lawrence and D. G. Whittten, *Photochem. Photobiol.*, **64**, 923 (1966).

32 D. M. Guldi and K.-D. Asmus, *J. Am. Chem. Soc.*, **119**, 5744 (1997).

33 M. E. El-Khouly, M. Fujitsuka, and O. Ito, *J. Porphyin. Phthalocyanin.*, **4**, 590 (2000).

34 N. Barboy and J. Feitelson, *J. Phys. Chem.*, **88**, 1065 (1984).